Chemical Science

ROYAL SOCIETY OF CHEMISTRY

EDGE ARTICLE

View Article Online
View Journal | View Issue

Cite this: *Chem. Sci.*, 2022, **13**, 9277

All publication charges for this article have been paid for by the Royal Society of Chemistry

Reversing the dendrite growth direction and eliminating the concentration polarization *via* an internal electric field for stable lithium metal anodes†

Yue Ma,[ac] Feng Wu,[abc] Nan Chen,*[ac] Yitian Ma,[a] Chao Yang,[d] Yanxin Shang,[ac] Hanxiao Liu,[ac] Li Li[abc] and Renjie Chen *[abc]

Lithium (Li) dendrite growth is a long-standing challenge leading to short cycle life and safety issues in Li metal batteries. Li dendrite growth is kinetically controlled by ion transport, the concentration gradient, and the local electric field. In this study, an internal electric field is generated between the anode and Au-modified separator to eliminate the concentration gradient of Li^+. The Li–Au alloy is formed during the first cycle of Li plating/stripping, which causes Li^+ deposition on the Au-modified side and lithium anode electrode, reversing the lithium dendrite growth direction. The electrically coupled Li metal electrode and Au-modified film create a uniform electric potential and Li^+ concentration distribution, resulting in reduced concentration polarization and stable Li deposition. As a result, the Au-modified separator improves the lifespan of Li||Li batteries; the Li||$LiFePO_4$ cells show excellent capacity retention (>97.8% after 350 cycles), and Li||$LiNi_{0.8}Co_{0.1}Mn_{0.1}O_2$ cells deliver 75.1% capacity retention for more than 300 cycles at 1C rate. This strategy offers an efficient approach for commercial application in advanced metallic Li batteries.

Received 14th June 2022
Accepted 10th July 2022

DOI: 10.1039/d2sc03313e

rsc.li/chemical-science

1. Introduction

As one of the ideal anode materials for high energy density batteries, lithium (Li) metal has received enormous attention due to its high theoretical specific capacity (3860 mA h g^{-1}) and low electrochemical potential (−3.04 V *vs.* the standard hydrogen electrode).[1–3] However, Li metal faces the challenge of uncontrollable growth of Li dendrites during the continuous cycling process, which generates safety concerns and capacity fading, restraining its application. The key to achieving safety and extended circular life in Li metal batteries (LMBs) is the control of the concentration polarization and reversal of the growth direction of dendritic Li. Because the ion diffusion rate in the electrolyte is lower than the electrochemical reaction rate at high current densities, concentration polarization occurs, resulting in nonuniform ion diffusion and the formation of Li dendrites.[4] In addition, due to nonuniform ion diffusion, Li dendrites grow towards the separator and pierce the separator, further causing an internal short circuit in the battery, and even explosions.[5,6]

Recently, various strategies have been explored to homogenize Li^+ diffusion. An effective approach for controlling the solid electrolyte interphase (SEI) layer is by changing the composition,[7,8] building a stable structure,[9] and improving the mechanical properties and diffusion rate of Li^+.[10–13] It has been demonstrated that lithium fluoride (LiF)[14] and lithium nitrate (Li_3N)[15,16] can enhance mechanical and electrochemical stability. Some reports have also introduced Li–M alloys to guide uniform deposition of Li^+ for the stabilization of Li metal.[17–20] These alloys act as a conductor for fast Li^+ diffusion while also prevent Li^+ ion reduction on the surface of the Li anode, which effectively suppresses the growth of Li dendrites. During the cycling process, however, the volume expansion of the Li metal anode may damage the SEI layer. Another viable technique is to improve Li^+ transport by creating an electrolyte with single-ion conduction or an anion-immobilized electrolyte.[21–23] This method avoids concentration polarization, unnecessary parasitic reactions with the electrode, and the growth of Li dendrites caused by freely moving anions. Unfortunately, single-ion or anion-immobilized electrolytes decrease the conductivity and increase the ohmic polarization of the batteries.

[a]*Beijing Key Laboratory of Environmental Science and Engineering, School of Materials Science and Engineering, Beijing Institute of Technology, Beijing 100081, China. E-mail: chenrj@bit.edu.cn; chenn@bit.edu.cn*

[b]*Collaborative Innovation Center of Electric Vehicles in Beijing, Beijing 100081, China*

[c]*Advanced Technology Research Institute, Beijing Institute of Technology, Jinan 250300, China*

[d]*Helmholtz Zentrum Berlin Mat & Energie, D-14109 Berlin, Germany*

† Electronic supplementary information (ESI) available: Experimental section, SEM characterization, XPS profiles, more electrochemical results, and Table S1. See https://doi.org/10.1039/d2sc03313e

In the abovementioned methods, Li dendrites still grow along the negative electrode toward the separator during the continuous Li plating/stripping process. The safety hazards have not been eliminated. The direction of Li dendrite growth is related to cation exhaustion (ion concentration polarization) and electric field aggregation (charge distribution polarization) at the deposition sites.[24–26] The dendritic structure of Li is easily generated under the circumstances of diffusion limitation. When the reaction rate of the chemical substance is greater than the diffusion rate, the concentration gradient is formed before crystal growth. The gradient results in an unstable crystal surface and further leads to the formation of dendritic structure, which has been confirmed by theoretical and experimental studies.[27] In addition, the stored charge and the distribution of the electric field on the anode/electrolyte interface are key factors affecting the morphology of Li deposition.[28] The inhomogeneous distribution of the charge field and electric field is likely to aggravate dendritic Li growth. As a result, the key to limiting dendritic Li toxicity is to improve the transport and uniform distribution of Li^+ ions.[13,29]

Here, we reported a simple approach to control the Li dendrite growth direction by decorating gold (Au) nanoparticles on one side of the separator *via* the magnetron sputtering method. Lithiophilic Au nanoparticles are utilized as a separator modifier for uniform Li deposition with a lower Gibbs free energy, which helps protect the anode from Li dendrites.[30] In the first cycle, Li and Au form a Li–Au alloy layer, and the internal electric field is generated between the modified side of the separator and negative electrode, which creates a further uniform Li^+ distribution and eliminates the ion concentration gradient. The Au-modified separator effectively restrains the elongation of dendritic Li during the cycling process. Correspondingly, the effect of the Au-modified separator on low interface impedance, high coulombic efficiency (CE), and long cycle life of Li‖Cu, Li‖Li, Li‖$LiFePO_4$, and Li‖$LiNi_{0.8}Co_{0.1}Mn_{0.1}O_2$ batteries are investigated.

2. Results and discussion

2.1 Morphology and structural characterization

A schematic illustration of the preparation of a Au-modified separator is shown in Fig. S1.† The magnetron sputtering method is used for surface modification. The separator is installed on a DC magnetron sputtering system for the deposition of metallic Au. During the preparation process, an ionized Ar^+ beam is incident on the Au target and generates Au atoms. The Au atoms flowing to the separator substrate are suppressed by the equilibrium magnetron field, which recombines them into Au nanoparticles. We first explore the effects of different sputtering times on the electrochemical properties of Li‖Cu cells. The cycling stability of Li‖Cu batteries with a sputtering time ranging from 10 to 40 s was evaluated at 2 mA cm^{-2}. As observed in Fig. S2† the Au-modified separator with sputtering time of 30 s shows a higher CE of about 93% over 150 cycles.

Fig. 1a shows the optical images of the Au-modified and blank separators. The modified side of the separator is a metallic light blue colour and the blank separator is white. Scanning electron microscopy (SEM) images reveal that Au nanoparticles are uniformly distributed on the surface of the separator, and the modified separator maintains a porous structure to allow Li^+ diffusion (Fig. 1b, c and S3a†). The surface SEM image also shows that no distinct change is observed for the back side, suggesting that the functional integrality and porous structure of the Au-modified separator is maintained during the sputtering process (Fig. S3b†).

The cross-sectional views of the Au-modified separator show that the Au nanoparticles create a thin film with a sputtering depth of 2.2 μm (Fig. 1d and S3c†). Au nanoparticles connect to the separator and distribute evenly, according to mapping images of the elements Au and C (Fig. 1e and S4†). The X-ray photoelectron spectroscopy (XPS) spectrum of the Au-modified separator (Au coated side) shows two strong peaks for Au 4f at 83.8 and 87.5 eV, indicating that the loaded nanoparticles are simple substance Au without other reactions (Fig. 1f). Atomic force microscopy (AFM) shows the uniform distribution of Au particles with an average diameter of 20–30 nm (Fig. 1g and h). The electrolyte wettability of the separator is determined by contact angle measurement, and as shown in Fig. 1i, a smaller contact angle of 12.6° is observed for the Au-modified separator compared to that of the blank separator (~36°). The improved interfacial affinity toward electrolytes facilitates uniform Li^+ diffusion and reduces the concentration gradient of the anode/electrode interface.

2.2 Nucleation sites of the Au-modified separator

To investigate the chemical affinity of Au towards Li on the molecular scale, density functional theory (DFT) calculations were employed to probe the adsorption energy of a Li atom on Au and Cu, as shown in Fig. 2a and b. The Cu (001) and Au (001) surface slabs with four layers were constructed using the lattice constants. Through a 15 Å vacuum layer in the *z* direction, the slab is separated from the periodic images. The adsorption energy of Li on Au is −3.058 eV, which is much less than that on Cu (−2.410 eV). This demonstrates that Li prefers to be adsorbed and deposited on the Au surface. Obviously, Au nanoparticles have a lithiophilic characteristic, which facilitates Li deposition by acting as "seeds".

To further verify whether Li and Au combine to generate new substances, in-depth XPS characterization was performed to explore the composition evolution of Au on the modified separator after Li plating. As shown in Fig. 2c, major distinctive peaks in the Au 4f spectrum are found at 83.8, 84.5, 87.5, and 88.2 eV, showing that lithiation of the Au layer partially creates the Li–Au alloy during the Li plating process. Fig. 1f shows that the typical peaks of Au 4f are located at 83.8 and 87.5 eV, indicating that metallic Au is in an uncombined state. It is assumed that the peaks at 84.5 and 88.2 eV are attributed to the Li–Au alloy. As the Ar^+ sputtering time increased, the intensity of the Au 4f peak first increased and then decreased due to Li deposition on the surface of the modified separator. It can be concluded that the Au nanoparticles combine with Li to form an alloy layer, which has high Li^+ ion diffusion coefficients and

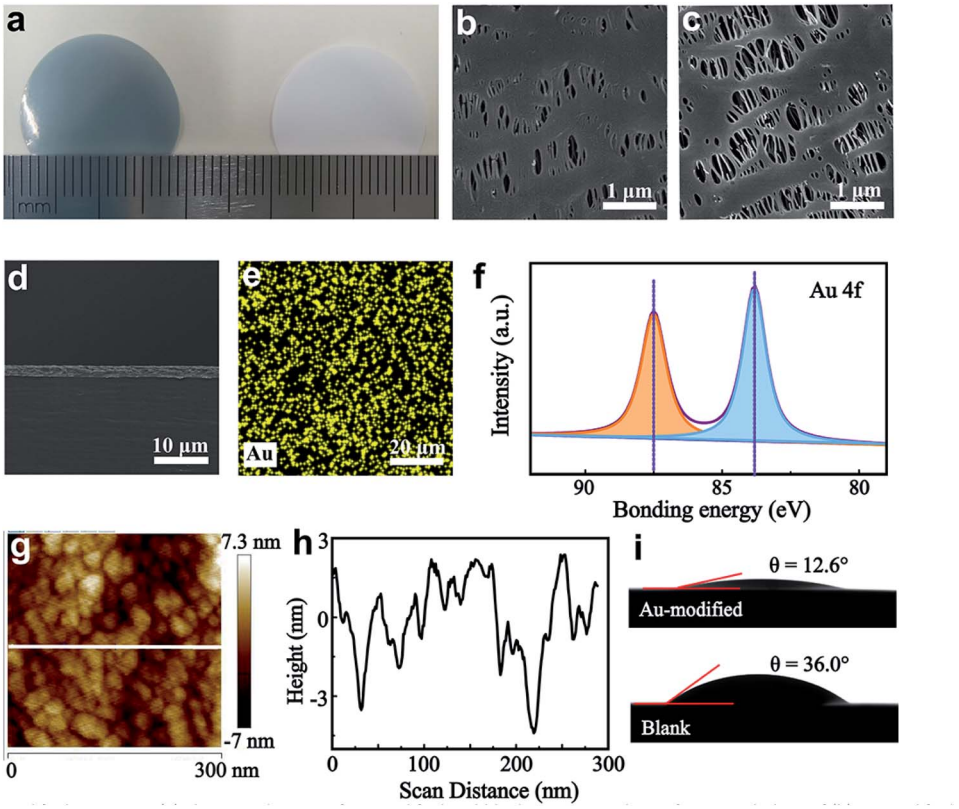

Fig. 1 Preparation of the Au-modified separator. (a) The optical image of Au-modified and blank separators. The surface morphology of the (b) Au-modified separator and (c) blank separator. (d) Side view SEM image and (e) EDS mapping images of the Au-modified separator. (f) Au 4f XPS spectra of the Au-modified separator (Au coated side). (g) Surface morphology AFM view of the Au-modified separator. (h) The height variation corresponding to the white line. (i) Wetting property of ether electrolyte on the Au-modified and blank separators.

keeps the bulk intact.[31] To further explore the stability of the Li–Au alloy layer, the Au-modified separator of Li||Cu batteries after 1 cycle and 10 cycles were characterized by SEM and XPS. As shown in Fig. S5,† the SEM images suggest that the surface morphology of the separator with a modified side remains stable without obvious change during the cycling process. In Fig. S6,† in-depth XPS spectra show the composition of the Li–Au alloy on the Au-modified separator after 1 cycle and 10 cycles with the Li stripping state. The results demonstrate the stability of the Au-modified separator in the cycling of Li||Cu cells.

To probe the effect of the Au-modified separator on Li deposition, we designed an electrically connected battery with a Li metal anode and a Au-modified film to ensure that the Au and Li anodes have the same potential difference. Synchrotron in-line phase contrast X-ray tomography was used[32,33] to record the Li microstructure after electrochemical deposition. The schematic diagram of the customized electrochemical cell is provided in Fig. 2d. And a Li||Li symmetric cell with an Au-modified separator was investigated. A detector system with a pixel size of 0.438 μm was employed to record all the tomographs. 2200 projections covering a rotation angle of 180° were measured. The region of view was about 1.7 × 1.2 mm^2 (length × height). Fig. 2e shows a cross-section image of the cell after deposition at 0.3 mA cm^{-2} for 10 h. Through light and dark interfaces, we can see the Li electrodes, separator, and Li deposition. The negative and positive Li electrodes are located at the bottom and top of the separator, respectively, with the Au-modified side facing the bottom lithium metal. Between the Au-modified separator and anode, there is an even and compact layer of Li deposition without significant protrusions. This happens because Li grows on both the Au-modified separator surface and the Li anode surface at the same time, changing the direction of Li deposition and resulting in dense, homogeneous Li. However, the blank separator deforms into an arch due to the significant stress resulting from the uneven deposition of lithium.[33] Fig. 2f shows that the Au-modified separator induces uniform lithium deposition from the top view.[32]

In addition to reversing the direction of Li deposition, a stable Li plating/stripping cycling process requires spatially homogeneous Li^+ transport between the electrolyte and the Li anode. To further investigate the function of the Au-modified separator on Li electrochemical deposition, we studied the Li||Cu half cells using SEM to monitor Li nucleation. The Li||Cu cells were assembled with the Au-modified side facing the Cu foil. A low current density (0.1 mA cm^{-2}) was used to study the nucleation process. After 15 min of deposition, Li is uniformly deposited on the lithiophilic Au particles of the separator (Fig. 2g). Simultaneously, the blank separator cell retained the original shape without any Li metal deposition on the surface (Fig. 2h), which further confirms that Au regulates the beginning of formation and outward growth of dendrites from the Au-modified separator surface toward the Li surface. The surface of

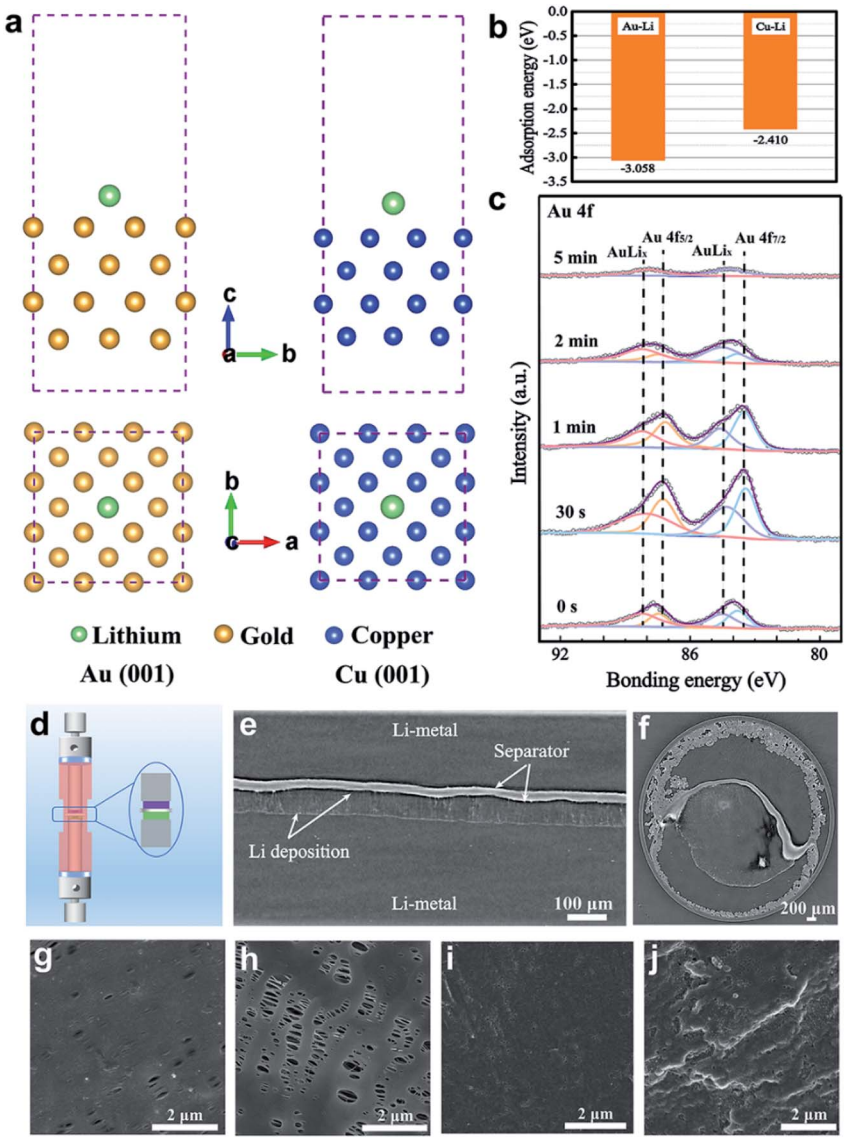

Fig. 2 Optimized structures of Li on (a) Au and Cu. (b) Adsorption energy of a Li atom with Au and Cu. (c) XPS spectra of the Au-modified separator after cycling. The bonding energy values using the adventitious C 1s peak at 284.6 eV. Synchrotron X-ray phase tomography of the Li||Li symmetric cell with the Au-modified separator after Li plating for 10 h at 0.3 mA cm^{-2}. (d) Schematic diagram of the electrochemical cell: polyamide-imide enclosure (pink), current collectors (light gray), sealing rings (blue), cathode material (purple), separator (silver gray), and anode material (green); (e) the cross-sectional part of the studied battery and (f) the horizontal plane view of the battery. A top view of (g) the Au-modified separator, (h) the blank separator and (i and j) the corresponding pieces of Cu foil after Li plating at 0.1 mA cm^{-2} for 15 min.

the Cu foil after deposition shows a flat and smooth Li film, without Li dendrite growth (Fig. 2i). This further demonstrates that Au nanoparticles are beneficial to the uniform deposition of Li^+. The Cu foil with the blank separator shows an uneven surface of mossy Li (Fig. 2j). The obvious change in morphology demonstrates the salutary effect of the Au nanoparticles on Li deposition, which may improve spatially uniform Li^+ transport between the electrolyte and Li anode by the effect of the internal electric field.

2.3 Mechanism of uniform Li^+ distribution

Au nanoparticles play a pivotal role in the Li deposition behaviour and superior electrochemical performance. To better understand the mechanism of the Au-modified separator, the distribution of the electric field and Li^+ concentration field was simulated and visualized *via* COMSOL Multiphysics simulation. The established numerical model includes a $LiFePO_4$ cathode, a Li anode, and a Au-modified separator with an operating voltage range of 2.7–4.2 V. The simulation system size is 40 × 20 μm (height × width) and the initial Li^+ concentration is 1 mol L^{-1}. The electric fields and ion concentration distribution after charging were simulated by COMSOL Multiphysics. Fig. 3a shows that the Au-modified separator exhibits a more homogeneous distribution of potential between the Li–Au alloy layer and Li metal anode, compared with the blank separator. From the curve, we can see that the potential distribution curve

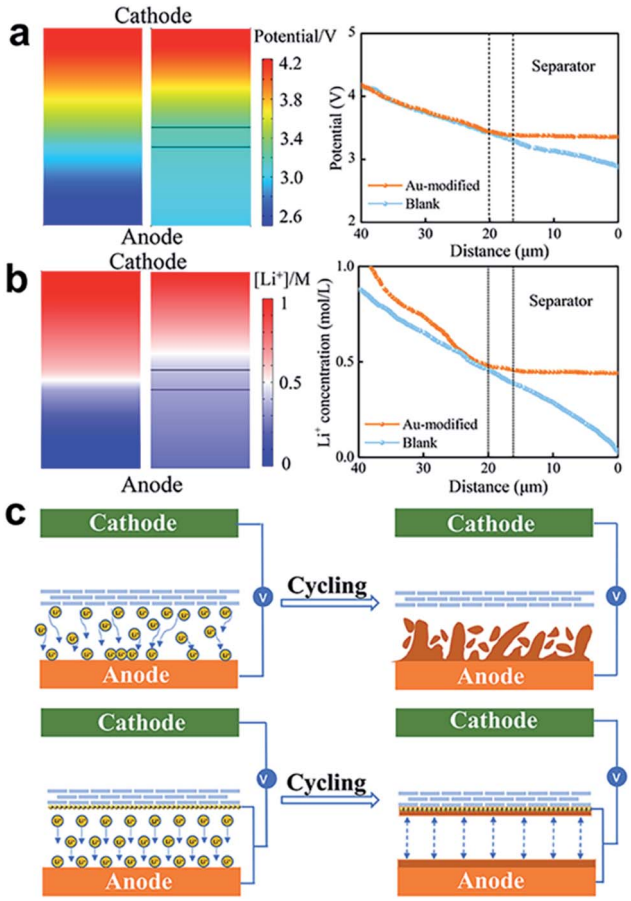

Fig. 3 (a) Simulation modes of electric field values of blank (left) and Au-modified (right) cells in the voltage range from 2.7 to 4.2 V. (b) Simulation results of Li^+ concentration distribution for Li||LFP cells using blank (left) and Au-modified (right) separators. (c) Schematic diagram of Li dendrite growth in batteries based on different separators.

continues to drop from 4.2 V and becomes stable after passing through the Au-modified separator, showing a uniform potential distribution of about 3.2–3.3 V between the separator and negative electrode. In contrast, the potential between the blank separator and negative electrode continues to drop from 3.3 V to 2.8 V. This can be attributed to an additional electric field due to the Li–Au alloy layer, which balances the charge between the separator and anode. Fig. 3b presents the Li^+ concentration distribution in the aforementioned electric fields. In the cell without a Li–Au alloy layer, 0.4 mol L^{-1} Li^+ concentration appears between the separator and negative electrode and gradually decreases to 0.1 mol L^{-1} on the Li electrode surface. This results in the fast growth of protrusions, thereby forming dendritic Li structures. The Li^+ concentration (~0.4 mol L^{-1}) attains an equal distribution without a concentration gradient after Au-modification, conducive to flat and smooth Li deposition without the formation of Li dendrites.

In summary, a reasonable Li deposition strategy is established *via* an effective modified separator, as shown in Fig. 3c. The Au metal is preferentially combined with Li to form an alloy layer, which is beneficial to the homogeneous distribution of the electric field between the separator and negative electrode, and further reduces the concentration gradient of Li^+ ions. This strategy is effective for inhibiting the formation of dendrites by encouraging uniform Li deposition.

2.4 Electrochemical performance

As depicted in Fig. 4a, Li||Cu cells with the Au-modified side facing the Cu electrode were assembled to explore the effect of Au nanoparticles on the deintercalation behavior of Li^+ ions. The nucleation overpotential is obtained by calculating the potential difference between the lowest tip voltage and voltage polarization, and it represents the energy barrier that Li^+ deposition needs to overcome.[2] Fig. 4b shows the voltage–capacity curves of Li deposited on the Cu substrate at 0.5 mA cm^{-2} with a capacity of 1 mA h cm^{-2}. The blank separator shows a high nucleation overpotential of 74.3 mV, while the nucleation overpotential of the Au-modified separator is only 21.4 mV. The lower nucleation overpotential indicates that metallic Au has a superior affinity for Li, and it is beneficial in homogenizing Li nucleation. This result is in accordance with the DFT calculation results.

Li||Cu cells with blank and Au-modified separators were fabricated to probe the stability of Au nanoparticles at 2 mA cm^{-2} with a capacity of 1 mA h cm^{-2}. Fig. 4c shows that the cell with a blank separator maintains a CE of about 87% for 80 cycles, which then declined rapidly. This capacity decay can be interpreted as a result of dendritic Li growth, which eventually causes a short circuit. In contrast, the cell with a Au-modified separator exhibits an extended cycling lifespan with a CE of about 93% after 150 cycles. Fig. S7† shows that the Au-modified separator retains a stable voltage polarization of 20 mV after 100 cycles. In comparison, the overpotentials of Li plating/stripping with the blank separator increase from 30.5 mV to 45.4 mV. The improvement of the electrochemical properties can be summarized in two aspects. On the one hand, the Au nanoparticles provide lithiophilic sites to guide Li deposition that is sufficient to stabilize the Li metal surface. The electrically coupled Li metal anode and Au-modified separator, on the other hand, provide an internal electric field that creates a uniform Li^+ concentration gradient.

To further verify the above point of view, we observed the surfaces of Li anodes with Au-modified and blank separators after the 30th cycle. Fig. 4d shows the smooth and dense deposited film that formed on the Cu foil of the Au-modified separator, while the Cu foil of the blank separator reveals a loose framework with a fragile surface (Fig. 4e). A dense and homogeneous Li deposition layer on the Cu substrate surface shows that the Au-modified separator effectively suppresses the elongation of Li dendrites.

Electrochemical impedance spectroscopy (EIS) analyses were performed to explore the effect of Au nanoparticles on the stability of symmetric Li||Li batteries. As shown in Fig. S8,† the impedance plots are composed of two parts of a depressed semicircle in the high frequency area and a slope in the low frequency area. The resistance value of the high frequency area at the intersection of the horizontal axis is the body resistance

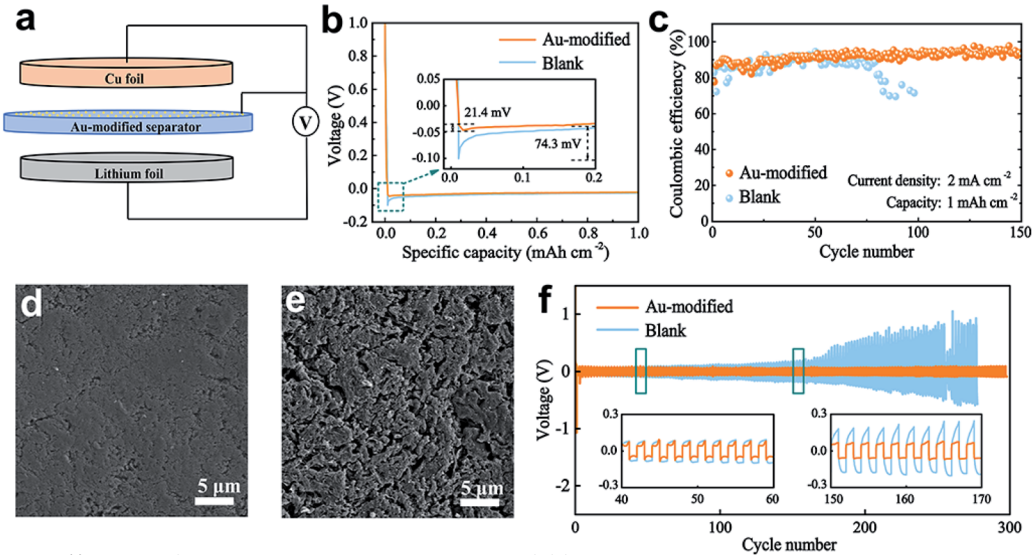

Fig. 4 (a) Illustration of the Li||Cu half cell (the Au-modified side facing the Cu foil). (b) Nucleation overpotential for Au-modified and blank cells at 1.0 mA cm^{-2}. (c) The CE of Li||Cu cells with blank and Au-modified separators at 2 mA cm^{-2} with a capacity of 1.0 mA h cm^{-2}. Surface morphology SEM images of the Li anode facing (d) Au-modified and (e) blank separators after the 30th cycle. (f) Voltage profiles for Li||Li symmetric cells with Au-modified and blank separators at 1.0 mA cm^{-2}.

R_b, and the semicircle diameter is R_{ct}, reflecting the ability of interfacial charge-transfer. In the beginning, the cell using an Au-modified separator presents a lower resistance (~50 Ω) than that using the blank separator (~160 Ω). Then, the resistance of the cells increased to 65 Ω and 210 Ω for the Au-modified and the blank separators, respectively, after 7 days of rest. After 15 days of rest, the impedance of the battery with the Au-modified separator slightly increased to 71 Ω while that of the battery with the blank separator continuously increased to 252 Ω. The ionic conductivity of the Au-modified and blank separators was based on EIS measurement of SS||SS cells assembled with different separators in the original state, as shown in Fig. S9.† The calculated ion conductivity of the Au-modified separator is around 1.10×10^{-3} S cm^{-1}, which is higher than that of the blank separator (0.96×10^{-3} S cm^{-1}). The results demonstrate that Au particles have a high ionic conductivity to allow Li^+ ions to diffuse quickly, implying that the Au-modified separator helps to lower the interface resistance. The Li^+ ion transference number (t_{Li^+}) of Li||Li symmetrical cells was measured by the Bruce–Vincent–Evans (BVE) technique to explore the effect of the Au-modified separator on the transportation of Li^+ ions. The chronoamperometry profile and the EIS spectrum are observed in Fig. S10,† revealing that the t_{Li^+} using the Au-modified separator is 0.65, while the value of t_{Li^+} using the blank separator is 0.49. The improved migration number of the Au-modified separator is beneficial in decreasing the concentration polarization in the charge/discharge process, which is consistent with the COMSOL simulation results. The cycling performance of symmetric Li||Li cells paired with Au-modified and pristine separators was evaluated at 1 mA cm^{-2} with a capacity of 1 mA h cm^{-2} to further highlight the influence of Au-modification on the cycling stability of Li metal. 1 M $LiPF_6$ + EC/DEC/EMC (1 : 1 : 1) was used as the electrolyte. The voltage–time profiles depicted in Fig. 4f show that the cell with a Au-modified separator maintains a stable overpotential of about 65 mV for more than 300 h, while the cell paired with a pristine separator exhibits a higher polarization hysteresis (>400 mV) after 170 h. The improved cycling stability of the battery demonstrates the favourable effect of Au nanoparticles on firm electrolyte/anode interphase formation.

2.5 Battery performance

To further explore the electrochemical properties of the Au-modified separator, $LiFePO_4$ (LFP) and $LiNi_{0.8}Co_{0.1}Mn_{0.1}O_2$ (NCM811) batteries were evaluated at 1C (1C = 170 mA h g^{-1} for Li||LFP and 1C = 180 mA h g^{-1} for Li||NCM811). Fig. 5a and b show the surface morphology views of Li anodes in the cells after 150 cycles. When the Au-modified separator is utilized, the Li anode has an even and homogeneous surface without any significant interfacial variations, indicating that the Au nanoparticles effectively guide Li deposition and reduce volume fluctuations. From the view in Fig. S11a,† the Li metal is also deposited on the modified separator, owing to the lithiophilicity of Au nanoparticles. In comparison, Fig. 5b shows a destroyed Li anode surface paired with a blank separator due to the unstable interface with continuous fracture and repair behaviour during the cycling process, and the porous and loose structure can consume more electrolyte, resulting in a reduced cycle life of the batteries. Fig. S11b† shows the surface view of the blank separator after 150 cycles. It is observed that the blank separator maintains the original porous structure without Li deposition on the surface.

The Li||LFP battery using the Au-modified separator displays a superior specific capacity of 123.2 mA h g^{-1}, and achieves a high-capacity retention of 97.8% after 350 cycles (Fig. 5c). Moreover, the battery retains stable voltage polarization under

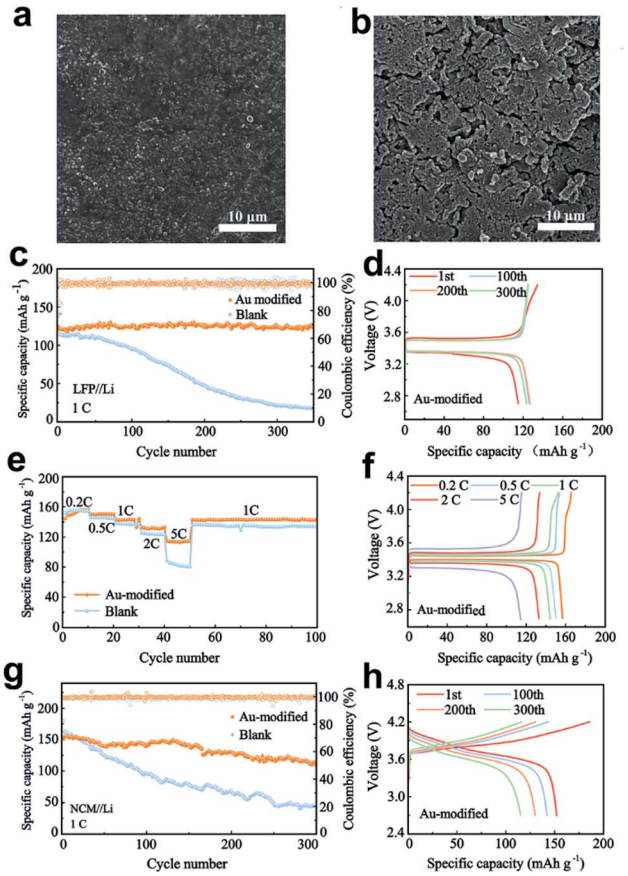

Fig. 5 Cell performance of the full cells with the Au-modified separator at 1C, in comparison with cells with the blank separator. (a and b) Top view SEM images of the Li anode in the Li||LFP cells after the 150th cycle. (c) Cycling stabilities of the Li||LFP cells with Au-modified and blank separators. (d) The charge/discharge profiles of Li||LFP with the Au-modified separator at different cycles. (e) Rate capabilities of the Li||LFP cells at different rates from 0.1C to 5C, and (f) the corresponding voltage profiles of Li||LFP with the Au-modified separator at different rates. (g) Cycling performances of the Li||NCM811 cells with two kinds of separators, and (h) the corresponding selected voltage curves of Li||NCM811 with the Au-modified separator at different cycles.

different cycling times (Fig. 5d), indicating the excellent stability of the interface in the cycling process. In comparison, the capacity of a battery paired with the blank separator persistently fades after 50 cycles, and drops to only 46 mA h g^{-1} after 200 cycles. The poor cycling performance is attributed to the increased voltage polarization of batteries (Fig. S12a†). Based on its merits, the full cell with the Au-modified separator also delivers excellent rate capability, as observed in Fig. 5e. At different rates, batteries paired with the Au-modified separator have higher specific capacity than those with the blank separator, especially at 5C. The corresponding charge–discharge profiles are depicted in Fig. 5f and S12b.† The results show that batteries with Au modification possess lower voltage polarization and higher specific capacity.

In addition, the Li||NCM811 cells with different separators were tested at a rate of 1C (Fig. 5g). After 300 cycles, the Li|Au|NCM cell maintains a superior specific capacity of 114.4 mA h g^{-1}, achieving a capacity retention of about 75.1%. However, the capacity of a battery with the blank separator continuously fades after 50 cycles and drops to only 50.8 mA h g^{-1}. The corresponding voltage–capacity profiles are presented in Fig. 5h and S13.† The batteries retain lower voltage polarization and higher specific capacity in the cycling process, suggesting that the Au-modified separator regulates Li deposition and inhibits the growth of dendritic Li. In contrast, the batteries paired with the blank separator exhibit increased voltage polarization and much lower capacity retention due to the unstable interface and dendrite growth.

Therefore, the results of cycling performance and rate capacities are consistent for Li||Cu cells and Li||Li cells, which demonstrates that the Au-modified separator can efficiently enhance the cycling stability. Hence, the above results indicate that Au nanoparticles are beneficial for guiding uniform Li deposition.

3. Conclusions

In summary, we report a facile separator that tackles problematic dendritic Li growth through controllable modification of Au nanoparticles *via* the DC magnetron sputtering method. Lithiophilic Au nanoparticles are utilized as a separator modifier for uniform Li electrodeposition with a lower Gibbs free energy. Based on this lithiophilic separator, the growth direction of Li dendrites is changed from the traditional "bottom-up" to "top-down". This reduces the risk of Li dendrites piercing the separator during long-term cycling and improves the battery's safety performance. In addition, Au nanoparticles can react with Li during the first cycle to form a Li–Au alloy. An internal electric field is constructed between the Li–Au alloy and Li anode. This internal electric field facilitates the homogeneous distribution of Li^+ ions between the separator and electrode, weakens the concentration gradient, and uniformly deposits Li^+ on the anode. As a result, the assembled Li||Cu cell exhibits an improved CE of 93.9% for more than 150 cycles, and the Li||LFP battery shows an excellent capacity retention of 97.8% over 350 cycles at a rate of 1C. Additionally, the Li||NCM811 battery achieves a capacity retention of 75.1% for more than 300 cycles at 1C. These cycling performances reveal the beneficial effect of Au nanoparticles, which enable the homogeneous deposition of Li. In light of the aforementioned benefits, the Au-modified separator is being considered as a potential candidate for practical applications in high-energy rechargeable LMBs.

Data availability

Detailed experimental procedures and computational methods are included in the ESI.†

Author contributions

Yue Ma and Nan Chen conceived and designed this study. Yue Ma, Yitian Ma, Chao Yang, and Hanxiao Liu conducted the material preparation, characterization studies, and electrochemical measurements. Yue Ma analyzed the data and wrote

the manuscript. The manuscript was discussed and revised by all authors.

Conflicts of interest

There are no conflicts to declare.

Acknowledgements

This work was supported by the Key Research and Development Program of Shandong Province (2021CXGC010401), National Science Foundation of China (52002023), Beijing Institute of Technology Research Fund Program for Young Scholars and Beijing Outstanding Young Scientists Program (BJJWZYJH01201910007023).

Notes and references

1 A. Hagopian, M. L. Doublet and J. S. Filhol, *Energy Environ. Sci.*, 2020, **13**, 5186–5197.
2 C. J. Huang, B. Thirumalraj, H. C. Tao, K. N. Shitaw, H. Sutiono, T. T. Hagos, T. T. Beyene, L. M. Kuo, C. C. Wang, S. H. Wu, W. N. Su and B. J. Hwang, *Nat. Commun.*, 2021, **12**, 1452.
3 Y. X. Huang, F. Wu and R. J. Chen, *Natl. Sci. Rev.*, 2020, **7**, 1367–1386.
4 X. Zhang, Y. Yang and Z. Zhou, *Chem. Soc. Rev.*, 2020, **49**, 3040.
5 Y. Chen, M. Yue, C. Liu, H. Zhang, Y. Yu, X. Li and H. Zhang, *Adv. Funct. Mater.*, 2019, **29**, 1806752.
6 L. Ma, J. Cui, S. Yao, X. Liu, Y. Luo, X. Shen and J. K. Kim, *Energy Storage Mater.*, 2020, **27**, 522–554.
7 Y. Gao, Z. Yan, J. L. Gray, X. He, D. Wang, T. Chen, Q. Huang, Y. C. Li, H. Wang, S. H. Kim, T. E. Mallouk and D. Wang, *Nat. Mater.*, 2019, **18**, 384–389.
8 C. Z. Wang, A. Wang, L. X. Ren, X. Z. Guan, D. H. Wang, A. Dong, C. Y. Zhang, G. J. Li and J. Y. Luo, *Adv. Funct. Mater.*, 2019, **29**, 1905940.
9 J. Wang, J. Yang, Q. Xiao, J. Zhang, T. Li, L. Jia, Z. Wang, S. Cheng, L. Li, M. Liu, H. Liu, H. Lin and Y. Zhang, *Adv. Funct. Mater.*, 2020, **317**, 2007434.
10 H. Chen, A. Pei, D. Lin, J. Xie, A. Yang, J. Xu, K. Lin, J. Wang, H. Wang, F. Shi, D. Boyle and Y. Cui, *Adv. Energy Mater.*, 2019, **9**, 1900858.
11 H. Dai, J. Dong, M. Wu, Q. Hu, D. Wang, L. Zuin, N. Chen, C. Lai, G. Zhang and S. Sun, *Angew. Chem., Int. Ed. Engl.*, 2021, **133**, 20005.
12 T. Chen, F. Meng, Z. Zhang, J. Liang, Y. Hu, W. Kong, X. L. Zhang and Z. Jin, *Nano Energy*, 2020, **76**, 105068.
13 C. Y. Zhang, S. Liu, G. J. Li, C. J. Zhang, X. J. Liu and J. Y. Luo, *Adv. Mater.*, 2018, 1801328.
14 A. Hu, W. Chen, X. Du, Y. Hu, T. Lei, H. Wang, L. Xue, Y. Li, H. Sun, Y. Yan, J. Long, C. Shu, J. Zhu, B. Li, X. Wang and J. Xiong, *Energy Environ. Sci.*, 2021, **14**, 4115–4124.
15 Y. Luo, T. Li, H. Zhang, W. Liu, X. Zhang, J. Yan, H. Zhang and X. Li, *Angew. Chem., Int. Ed. Engl.*, 2021, **60**, 11718–11724.
16 Y. Liu, H. Su, M. Li, J. Xiang, X. Wu, Y. Zhong, X. Wang, X. Xia, C. Gu and J. Tu, *J. Mater. Chem. A*, 2021, **9**, 13531–13539.
17 H. Ye, Z. J. Zheng, H. R. Yao, S. C. Liu, T. T. Zuo, X. W. Wu, Y. X. Yin, N. W. Li, J. J. Gu, F. F. Cao and Y. G. Guo, *Angew. Chem., Int. Ed. Engl.*, 2019, **58**, 1094–1099.
18 S. Zhang, G. Yang, Z. Liu, S. Weng, X. Li, X. Wang, Y. Gao, Z. Wang and L. Chen, *ACS Energy Lett.*, 2021, **6**, 4118–4126.
19 X. Shen, G. Zhao, X. Yu, H. Huang, M. Wang and N. Zhang, *J. Mater. Chem. A*, 2021, **9**, 21695–21702.
20 J. Y. Cui, A. Wang, G. J. Li, D. H. Wang, D. Shu, A. P. Dong, G. L. Zhu, J. Y. Luo and B. D. Sun, *J. Mater. Chem. A*, 2020, **8**, 15399–15416.
21 K. S. Oh, J. H. Kim, S. H. Kim, D. Oh, S. P. Han, K. Jung, Z. Wang, L. Shi, Y. Su, T. Yim, S. Yuan and S. Y. Lee, *Adv. Energy Mater.*, 2021, **11**, 2101813.
22 K. Liu, S. Jiang, T. L. Dzwiniel, H. K. Kim, Z. Yu, N. L. Dietz Rago, J. J. Kim, T. T. Fister, J. Yang, Q. Liu, J. Gilbert, L. Cheng, V. Srinivasan, Z. Zhang and C. Liao, *ACS Appl. Mater. Interfaces*, 2020, **12**, 29162–29172.
23 C. Z. Zhao, X. Q. Zhang, X. B. Cheng, R. Zhang, R. Xu, P. Y. Chen, H. J. Peng, J. Q. Huang and Q. Zhang, *Proc. Natl. Acad. Sci. U. S. A.*, 2017, **114**, 11069–11074.
24 P. Bai, J. Guo, M. Wang, A. Kushima, L. Su, J. Li, F. Brushett and M. Bazant, *Joule*, 2018, **2**, 2434–2449.
25 X. Wang, W. Zeng, L. Hong, W. W. Xu, H. K. Yang, F. Wang, H. G. Duan, M. Tang and H. Q. Jiang, *Nat. Energy*, 2018, **3**, 227–235.
26 P. Zou, Y. Sui, H. Zhan, C. Wang, H. L. Xin, H. M. Cheng, F. Kang and C. Yang, *Chem. Rev.*, 2021, **121**, 5986–6056.
27 D. Lin, Y. Liu and Y. Cui, *Nat. Nanotechnol.*, 2017, **12**, 194–206.
28 L. X. Ren, A. Wang, X. Y. Zhang, G. J. Li, X. J. Liu and J. Y. Luo, *Adv. Energy Mater.*, 2020, **10**, 1902932.
29 Y. Ouyang, W. Zong, J. Wang, Z. Xu, L. L. Mo, F. L. Lai, Z. L. Xu, Y. E. Miao and T. X. Liu, *Energy Storage Mater.*, 2021, **42**, 68–77.
30 K. Yan, Z. D. Lu, H. W. Lee, F. Xiong, P. C. Hsu, Y. Z. Li, J. Zhao, S. Chu and Y. Cui, *Nat. Energy*, 2016, **1**, 16010.
31 L. L. Kong, L. Wang, Z. C. Ni, S. Liu, G. R. Li and X. P. Gao, *Adv. Funct. Mater.*, 2019, **29**, 1808756.
32 F. Sun, R. Moroni, K. Dong, H. Markotter, D. Zhou, A. Hilger, L. Zielke, R. Zengerle, S. Thiele, J. Banhart and I. Manke, *ACS Energy Lett.*, 2017, **2**, 94.
33 F. Sun, L. Zielke, H. Markotter, A. Hilger, D. Zhou, R. Moroni, R. Zengerle, S. Thiele, J. Banhart and I. Manke, *ACS Nano*, 2016, **10**, 7990–7997.